EARTH SURFACE PROCESSES AND LANDFORMS
Earth Surf. Process. Landforms **38**, 888–897 (2013)

Published online 31 January 2013 in Wiley Online Library
(wileyonlinelibrary.com) DOI: 10.1002/esp.3376

Historical analysis indicates seepage control on initiation of meandering

J. P. C. Eekhout,[1]* A. J. F. Hoitink[1] and B. Makaske[2]
[1] Hydrology and Quantitative Water Management Group, Wageningen University and Research Centre, Wageningen, The Netherlands
[2] Alterra, Wageningen University and Research Centre, Wageningen, The Netherlands

Received 12 June 2012; Revised 6 November 2012; Accepted 8 November 2012

*Correspondence to: Joris Eekhout, Hydrology and Quantitative Water Management Group, Wageningen University and Research Centre, PO Box 47, 6700 AA Wageningen, The Netherlands. E-mail: joris.eekhout@wur.nl

ESPL
Earth Surface Processes and Landforms

ABSTRACT: In analytical and numerical models of river meandering, initiation of meandering typically occurs uniformly along the streamwise coordinate in the channel. Based on a historical analysis of the Nierskanaal, here we show how and under which circumstances meandering has initiated in isolated sections of a channel. The Nierskanaal was constructed by the end of the 18th century, as a straight channel between the river Niers and the river Meuse. The purpose of this measure was to reduce flood risk in the downstream reaches of the river Niers. The banks on the Dutch part of the channel were left unprotected and developed into a morphodynamically active channel, featuring a meandering planform and valley incision. The planform development and incision process is analysed using topographic maps and airborne LiDAR data. Meandering initiated in three sections of the channel, where the channel sinuosity developed asynchronously. Sedimentary successions in the study area show layers of iron oxide, indicating groundwater seepage from aeolian river dunes and river deposits located nearby. Only at the spots where meandering has initiated iron oxide is found close to the surface level. This provides a clue that seepage triggered bank erosion by increasing moisture content of the banks. The isolated meandering sections expanded in the longitudinal direction. Valley incision has developed in the first decades after the construction of the channel, and diminished after a gravel layer was reached. Gravel was deposited in the downstream half of the channel bed, acting as an armouring layer. The spatial variation in meandering behaviour, as observed in the Nierskanaal, justifies efforts to implement the influence of floodplain heterogeneity and the effect of seepage on bank erosion in meander models. Copyright © 2013 John Wiley & Sons, Ltd.

KEYWORDS: initiation of meandering; seepage; river meandering; valley incision; historical sources

Introduction

River meander dynamics has intrigued many scientists throughout history. Recently, the interest in meander behaviour has intensified in the context of stream restoration projects aiming at restoring sinuous/meandering planforms and subsequent free morphological behaviour. Meander dynamics have been studied by applying analytical and numerical models. Ikeda *et al.* (1981) was among the first to develop a meander model that includes a description of the river flow and bed topography, simulating lateral channel shift. Their modelling approach was the basis of a number of subsequent meander models (e.g. Richardson, 2002; Abad and García, 2006; Coulthard and Van de Wiel, 2006). Blondeaux and Seminara (1985) and Struiksma *et al.* (1985) showed the importance of coupling the hydrodynamic equations with the conservation equation of sediment. This has led to meander migration models based on the full Saint-Venant equations (e.g. Crosato, 1987; Johannesson and Parker, 1989; Howard, 1996; Stølum, 1996; Sun *et al.*, 1996, 2001; Zolezzi and Seminara, 2001). In many of these models, which capture much of our current understanding about river morphology, meandering initiates uniformly along the streamwise coordinate. Based on a historical analysis, this contribution shows how meandering initiates in isolated sections along a channel, which can be related to floodplain heterogeneity.

Initiation of meandering has been attributed to two types of instability responses, unified by Blondeaux and Seminara (1985). The first to emerge was the so-called *bar theory*, which considers the stability of the alluvial bed and shows that small perturbations in the channel bed may develop into an alternate bar pattern (e.g. Hansen, 1967; Callander, 1969; Engelund, 1970). At the pools between the bars, near-bank flow velocities and water depths are higher, resulting in localized bank erosion, and hence a sinuous channel planform. *Bend theory* (Ikeda *et al.*, 1981) considers the planform instability of a straight channel and shows that a small perturbation of the channel centreline may lead to the development of meanders.

In most meander models developed so far, the migration rate is obtained by multiplying the near-bank excess flow velocity by a dimensionless erosion coefficient, which depends on the physical properties of the banks and their vegetation cover. The value of the erosion coefficient also depends on the numerical solution of the model (Crosato, 2007). For cases where field data are available, the coefficient is obtained empirically

based on calibration, using observed erosion rates. These erosion rates are either measured in the field or obtained by remote sensing data, e.g. aerial/satellite imagery. Calibration of the erosion coefficient is a challenge, considering the heterogeneity of floodplain soils, the presence of vegetation and other causes of spatial variation. Often, observed erosion rates from field studies are lacking.

Recently, several studies have focused on the relation between floodplain characteristics and meander dynamics. Van Balen *et al.* (2008) addressed the spatial heterogeneity of bank erosion in a meander migration model through the dependence of erosion rates on seepage flow in the banks. They showed a positive feedback may exist between seepage rates and bank migration: bank migration focuses groundwater flow, causing more seepage at the bank, which in turn enhances migration rates. Güneralp and Rhoads (2011) showed that heterogeneity in erosional resistance of the floodplain has a major influence on meander evolution. Motta *et al.* (2012) presented an analytical meander model based on the work by Ikeda *et al.* (1981), coupled to a physics-based bank erosion module (Langendoen and Alonso, 2008; Langendoen and Simon, 2008). They simulated features of planform behaviour that are commonly observed in nature, but previously could not be simulated using the constant erosion coefficient approach. Following Güneralp and Rhoads (2011), Motta *et al.* (2012) extended their model for the case of heterogeneous floodplain sediments. They concluded that complexity of the floodplain sediments contributes to the complexity of the channel planform.

Laboratory experiments have shown that it is possible to create a physical scale model of a meandering planform. Federici and Paola (2003) presented an experiment in which a meandering channel formed after some time. However, the meandering channel eventually evolved into a braided river pattern due to the lack of cohesion of the bank material. Therefore, the type of sediment plays a major role in the creation of meanders under laboratory conditions. Several sediment mixtures have been used, which all have a different way of adding cohesion to the floodplain material. In the past, solely cohesive material was used to create meanders in the lab (Friedkin, 1945; Schumm and Khan, 1971; Smith, 1998). More recently, mixtures of cohesive and non-cohesive sediment were explored to achieve realistic river meandering in laboratory flumes, using for example silica flour (Peakall *et al.*, 2007; Van Dijk *et al.*, 2012). Braudrick *et al.* (2009) used alfalfa sprouts to obtain a stable meandering planform. Both Peakall *et al.* (2007) and Braudrick *et al.* (2009) also introduced an initial perturbation in the channel planform.

Considering the calibration requirements of bank erosion parameters in mechanistic models, and scaling issues in laboratory experiments, field studies and historical reconstructions are crucial in studying the timescales and spatial development characterizing channel development. Long-term field-scale reconstructions of meandering channels are limited by the availability of historical sources to reconstruct the meandering planform, especially before 1900. Planform reconstructions are mainly based on historical topographic maps (Pišút, 2002; Uribelarrea *et al.*, 2003; Timár *et al.*, 2008; Church and Rice, 2009; Hooke and Yorke, 2010) and aerial photographs (Warburton *et al.*, 2002; Uribelarrea *et al.*, 2003; Bartley *et al.*, 2008; Church and Rice, 2009; Hooke and Yorke, 2010), of which the latter are often available from the 1940s onwards. Recently, airborne LiDAR and satellite imagery have become customary tools for geomorphological studies (Charlton *et al.*, 2003; Timár *et al.*, 2008), offering a means of recognizing historical channel patterns (Seker *et al.*, 2005; Notebaert *et al.*, 2009).

The objective of this study is to contribute to the knowledge about the role of floodplain heterogeneity on the spatiotemporal developments of meander formation, by making a historical reconstruction of the meander behaviour and incision development of an initially straight channel.

Study Area

Engineering works

The artificial channel under study, named Nierskanaal and centred at 51° 30′ 54″ N, 6° 11′ 14″ E, was constructed by the Prussians by the end of the 18th century, probably around 1770. The channel is located on the Dutch–German border in the southeastern part of the Netherlands and runs from the river Niers in Germany to the river Meuse in the Netherlands (Figure 1). The purpose of the channel was to lower peak discharges in the downstream reaches of the river Niers, which is a tributary of the river Meuse. At the inlet of the channel, a weir controls the inflow of water. Inflow of water is regulated by an agreement between the Dutch and German water authorities, settled in 1952. Discharge is measured close to the inlet. Discharge data from 1971 to 2008 were used to calculate a mean daily discharge of $0.71\,m^3\,s^{-1}$ and an average yearly peak discharge of $4.07\,m^3\,s^{-1}$.

The total length of the channel is 13.3 km. The banks of the German part of the channel were protected, to prevent lateral developments, whereas the Dutch part developed into a morphodynamically active meandering channel. The Dutch part, in turn, can be subdivided into two parts. Between the early 1900s and 1940s, the banks of the upstream part became protected with bank revetments. At present, those bank revetments are still visible at some locations (see Figure 3e). Two bridges are present in the upstream section: one at the Dutch–German border and one approximately 0.5 km downstream from the border. The downstream part of the study reach can be considered undisturbed regarding its geomorphology, with no erosion or flood controls, and the presence of only one bridge near the mouth of the channel where it debouches into the river Meuse. The study area is located in a deciduous forest, surrounded by several agricultural fields.

Geology

Figure 1 shows the main geomorphological units of the study area, in a plan view (panel b), and the related sedimentary units, in a cross-section (panel c). The sedimentary units are divided into aeolian, Rhine and Meuse deposits. The Pleistocene Rhine and Meuse terrace deposits mainly consist of coarse sand and gravel. The recent river deposits in the floodplains along the rivers Meuse and Niers predominantly consist of clay. The aeolian deposits consist of fine to coarse sand. Figure 1b shows that the German part of the study area is mainly influenced by the river Rhine. Here, the channel follows a valley occupied by an abandoned (lower) Rhine terrace, between middle and upper Rhine terrace remnants. The upper Rhine terrace remnant explains why the channel was not constructed in a straight line from Geldern to the Meuse. The channel follows the northern edge of the upper Rhine terrace. On Dutch territory, the channel predominantly has scoured into Meuse terrace deposits. The channel flows across a middle/upper terrace, and crosses an area of aeolian sand dune deposits, before debouching into the river Meuse.

The study reach is located in the Dutch part of the channel with a length of 3.8 km, extending from the German–Dutch border to the outflow in the river Meuse. Here, the channel gradient varies between $0.48\,m\,km^{-1}$ in the upstream section and $3.8\,m\,km^{-1}$ near the mouth. The channel gradients in the

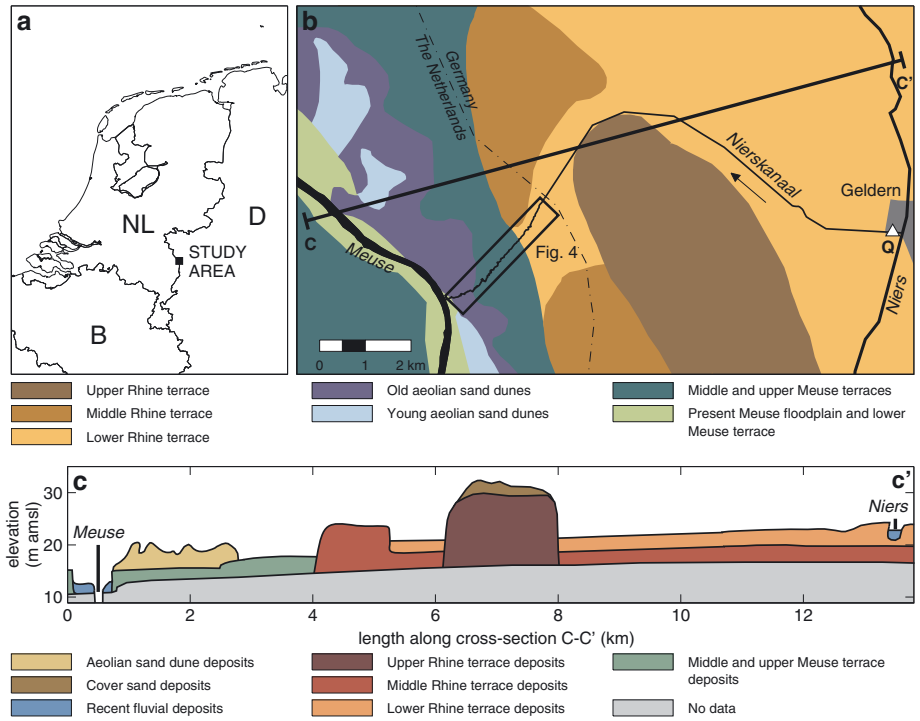

Figure 1. Overview of the study area with (a) the location of the study area on the German–Dutch border, (b) a geomorphological map of the study area, where Q indicates the location of the discharge station and the rectangle indicates the location of Figure 4, and (c) a schematic cross-section showing sedimentary units across transect C-C' in panel (b). The terrace denominations 'upper', 'middle' and 'lower' in panels (b) and (c) are used as relative indications of terrace levels in this figure and do not represent formal units in regional terrace classifications. Both (b) and (c) are adapted after Stiboka (1975), using data from Wolfert and De Lange (1990) and Van den Berg (1996). This figure is available in colour online at wileyonlinelibrary.com/journal/espl

upstream section are comparable to those in the Niers (Kasse *et al.*, 2005) and to the lowland streams analysed by Wolfert (2001). The channel gradients in the downstream section correspond to the small streams found in the hilly landscape in the province of Limburg in the southern part of the Netherlands (e.g. De Moor and Verstraeten, 2008). The average bankfull width and depth are 8.8 m and 1.2 m, respectively.

The bed material varies along the channel. In the upper section the bed material mainly consists of (coarse) sand, with a median grain size of 0.80 mm (see Figure 2 for the grain size distributions). There are several weakly developed point bars located in the inner bends. The bed material in this section is typical for Dutch lowland streams, which mainly consists of sand (Wolfert, 2001). In the downstream section, the bed material gradually becomes coarser and is dominated by gravel, with a median grain size of 18.1 mm (Figure 2). The in-channel morphology changes in downstream direction along the channel. A total of 67 gravel bars have been identified in the downstream section of the channel, which are only exposed during periods of low flow. Figure 3a, b show examples of the point bars and mid-channel bars.

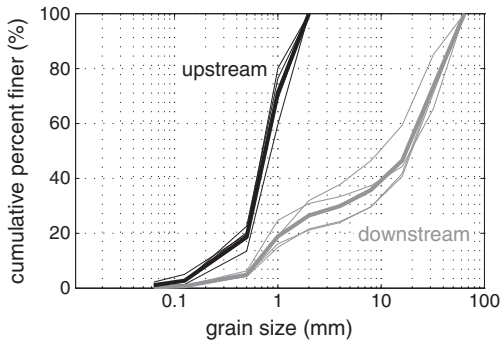

Figure 2. Grain size distributions from bed material samples from four locations in the upstream part (black lines) and four locations in the downstream part (grey lines). The thick lines denote the average for upstream and downstream samples, respectively.

At several locations along the valley edge, a clear view of the Pleistocene terrace deposits was obtained (see Figure 3d, g). At those locations, sediment textures and layer thicknesses were determined *in situ*. The USDA soil texture classification was used to differentiate between the different grain sizes, using a sand ruler. Figure 4 shows the sample locations in the study area. Figure 5 shows the sedimentary succession at 10 locations along the valley edge. The exposed deposits mainly consist of median to coarse sand. At eight locations, a thick (0.3–1.2 m) gravel layer and/or gravelly sand layer was visible. This is most likely the source of the current bed sediment, which consists of gravel in the downstream section of the channel. In a preliminary survey, red-brown coloured layers of sand were found at five locations along the valley edge, in which iron-rich groundwater oxidizes and turns red when it comes into contact with air. The groundwater comes into contact with air in the upper part of the groundwater column, and therefore the depth of the iron oxide gives an indication of the upper extent of the historical groundwater table.

Hydrology

The purpose of the channel was to reduce flood risk in the downstream reaches of the river Niers. This suggests that no water was led into the channel during low-flow periods, resulting in a non-natural discharge distribution. The Dutch and German water authorities, however, made an agreement

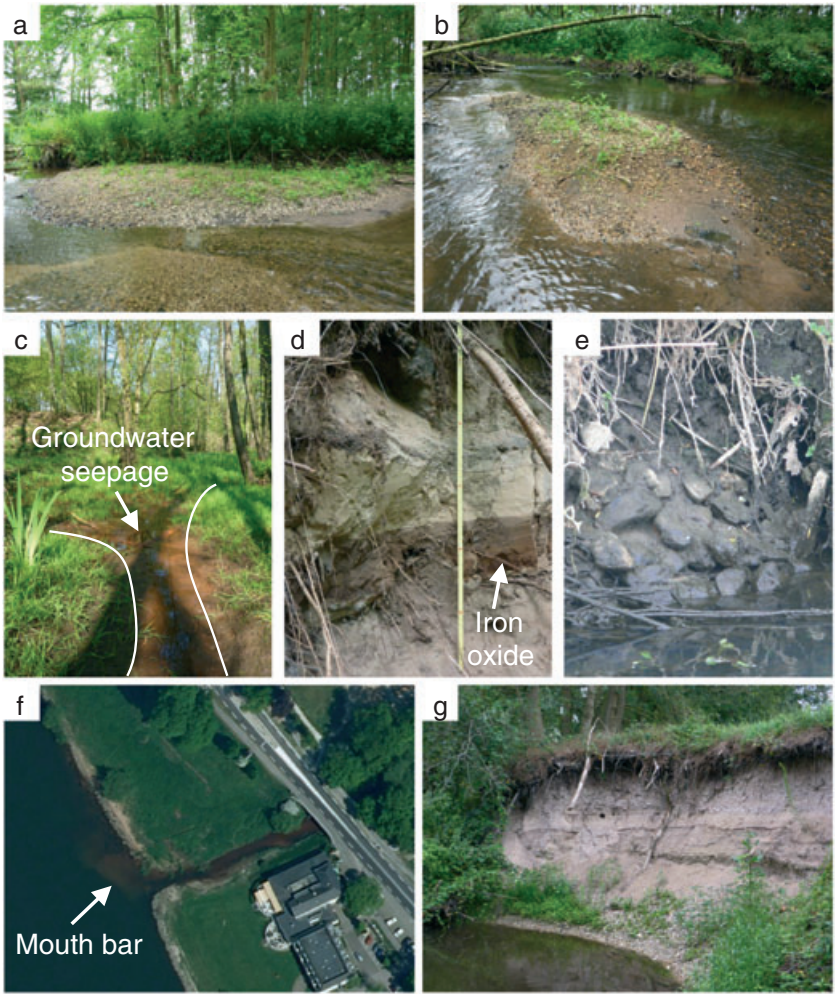

Figure 3. Photos of the study area, illustrating (a) a point bar, (b) a mid-channel bar, (c) the valley floor showing groundwater seepage, (d) a sedimentary succession showing a thick iron oxide layer (thickness 0.20 m), (e) the remnants of the bank protection, (f) an aerial photo (2008) of the area surrounding the confluence of the Nierskanaal and the river Meuse showing a mouth bar at the downstream side of the channel outlet (Copyright Eurosense BV, 2008) and (g) valley edge erosion (height of exposed sediments 2.5 m). See Figure 4 for photo locations. This figure is available in colour online at wileyonlinelibrary.com/journal/espl

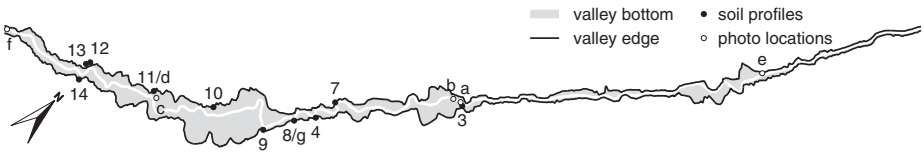

Figure 4. Locations of the exposed valley edges and photo locations corresponding to Figure 3. The extent of this figure corresponds to the rectangle in Figure 1. Flow is from right to left.

in 1952 which defined a minimum discharge of 0.5 $m^3 s^{-1}$ and a maximum of 7 $m^3 s^{-1}$. It is unknown how water discharge was distributed before that time.

Discharge time series of the Nierskanaal and Niers were compared to investigate the discharge distribution over the inlet of the channel and the downstream branch of the river Niers. Two discharge time series were used, both consisting of daily averaged discharge data. The discharge in the Nierskanaal was measured near the inlet (Figure 1). This discharge time series contains data covering the period between 1970 and 2008. The discharge in the river Niers was measured at the city of Goch between 1970 and 2006. For both data series, the monthly averaged discharge is shown in Figure 6. The figure also shows the 10%, 25%, 75% and 90% quantiles for every month.

As to the monthly average discharge (solid black line), both discharge time series show the same yearly pattern with high flows in January and February and low flows in August and September. The 25% and 75% quantiles also feature similar patterns for both data series. The 10% and 90% quantiles, however, show that the extremes in the river Niers are less pronounced than the extremes in the Nierskanaal. In other words, the peak discharges in January–February are relatively high in the Nierskanaal, compared to the river Niers. The same holds for low flows in the summer period. Thus the discharge in the Nierskanaal is relatively flashy.

The study area is located in the river Meuse catchment (36 000 km^2). The river Meuse has a length of 900 km and is a rain-fed river. It is an important waterway in western Europe, navigable from the North Sea up to France (Nienhuis, 2008). In the 19th century, navigation was impeded by sedimentation. Since the 19th century the river Meuse has been subject to measures aiming to improve navigation. This started with

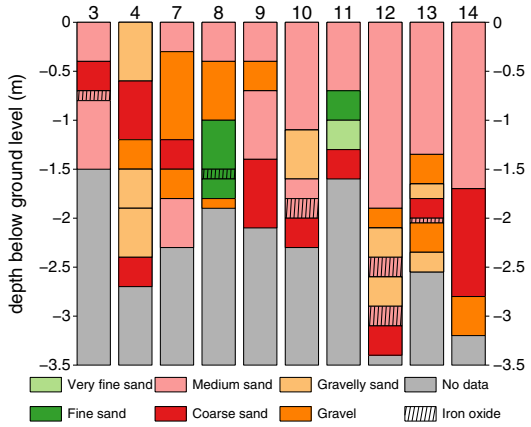

Figure 5. Sedimentary successions at 10 locations. See Figure 4 for the locations in the study area. Ground level corresponds to the level of the valley edge into which the channel has incised. This figure is available in colour online at wileyonlinelibrary.com/journal/espl

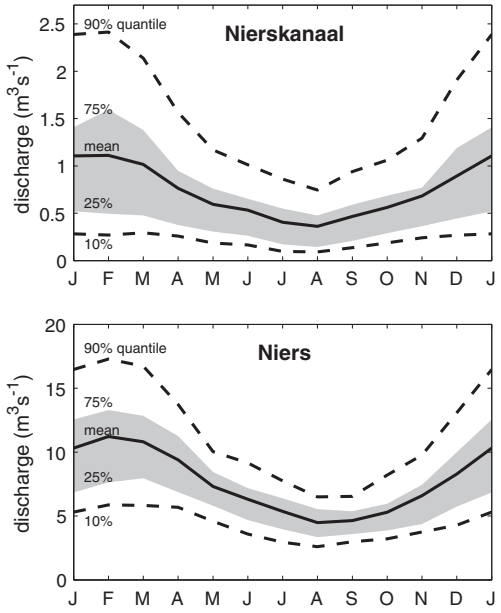

Figure 6. Monthly averaged discharge for the Nierskanaal (upper panel) and river Niers (lower panel). Indicated in grey are the 25% and 75% quantiles and with a dashed line the 10% and 90% quantiles.

dredging activities in the 19th century. In the 20th century, the measures became more rigorous. Several meanders were cut off, hundreds of groynes were built, lateral canals were constructed and, most importantly, from 1930 onwards the water level was fully controlled by six weirs in the Dutch part of the river Meuse (Nienhuis, 2008). All of this may have had an impact on the bed morphology of the Nierskanaal near the confluence with the river Meuse.

Water level data from the river Meuse were analysed to evaluate the dynamics of the downstream boundary (i.e. the downstream water surface level) of the Nierskanaal. At 14 locations water levels were measured daily. From these locations, two are in the vicinity of the confluence with the Nierskanaal, 4 km upstream and 6 km downstream from the mouth of the Nierskanaal, respectively. Both water level time series span a period from 1850 until the end of the 20th century. Figure 7 shows yearly averaged water levels in the period 1850–1984/1995 for these two locations. The figure clearly shows that the weirs were operational in the river Meuse from 1930 onwards, causing a water level increase of about 2 m from 1929 to 1930. Regression analysis shows there is a water level increase before the weirs were operational, for both locations. The cumulative water surface rise is equal to 0.31 m and 0.46 m for the upstream and downstream location, respectively. After the weirs became operational, the increasing trend is still visible, although less pronounced.

Bed level measurements have been performed from 1916 onwards, with irregular intervals between the surveys. These bathymetry data were collected along cross-river transects with a 100 m spacing, and width-averaged within the navigable section of the channel. Then, bed levels were averaged per river kilometre (Van Dongen and Meijer, 2008). Figure 7 shows the change in bed level of the river Meuse at the confluence with the Nierskanaal. Between 1930 and 1940, dredging operations were performed in this section of the river Meuse (Van Dongen and Meijer, 2008), causing a decrease of the bed level. Overall the bed level shows only minor changes between 1940 and 2010. We therefore conclude that the installation of the weirs in 1930 is the only substantial change at the downstream boundary of the Nierskanaal that has occurred since the construction of the channel. The installation of the weirs is therefore the main cause of the rise in water surface level at the confluence with the Nierskanaal.

Materials and Methods

Planform characteristics were derived from 12 historical maps, covering the period between 1806 and 2006. The oldest historical document available was the Tranchot map, based on data from a survey carried out around 1806. Four topographic military maps were used, dating from 1840 to 1936, and seven general topographic maps, dating from 1941 to 2006. Figure 8 shows an example of the topographic military map of 1895. The features that were derived from all maps are indicated in the

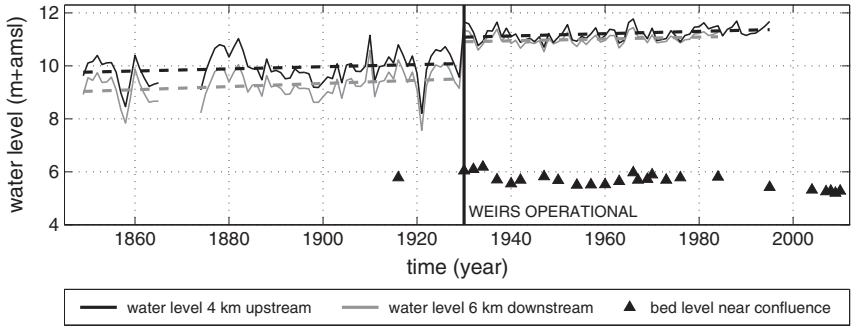

Figure 7. Historical yearly averaged water levels and bed levels from the river Meuse. The water level time series correspond to two locations near the confluence of the Nierskanaal, as indicated.

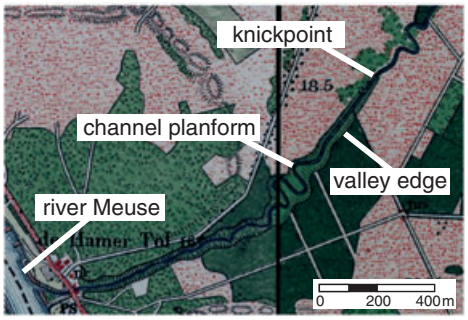

Figure 8. Topographic military map of 1895, showing features that were derived from the historical maps, viz. the channel centreline, the valley edges and a bed-level knickpoint marking the upstream end of the valley incision. This figure is available in colour online at wileyonlinelibrary.com/journal/espl

figure, including the channel centreline, the incised valley boundaries and the knickpoint of the bed level indicating the upstream end of valley incision. Table I lists the details of all historical maps. Each map was scanned at a resolution of 600 dpi and georeferenced using ESRI ArcGIS™. Centrelines were manually digitized, with an average node spacing of 10 m.

Figure 9 shows the channel centrelines derived from all 12 historical maps. Planform changes were evaluated based on total sinuosity S_{total}, computed by dividing the channel length L_{ch} by the valley axis length L_v. The valley axis is defined as the midline of the valley. An increase of S_{total} indicates an increase of channel length, which is the result of lateral migration of the channel. A decrease of total sinuosity in a meandering channel is mainly caused by meander cutoffs or by channel straightening through bank erosion. On the right-hand side of Figure 9 the total sinuosity is reported for the 12 channel centrelines. In the period between the construction of the channel until the mid 1930s, S_{total} increased. Between 1936 and 1955, a number of meander cutoffs occurred, which resulted in a decrease of S_{total}.

Table I. Characteristics of the historical topographic maps

Year	Map type	Scale
1806	Tranchot	1:25 000
1840	Topographic military map	1:50 000
1895	Topographic military map	1:50 000
1926	Topographic military map	1:50 000
1936	Topographic military map	1:50 000
1941	Topographic map	1:50 000
1955	Topographic map	1:25 000
1965	Topographic map	1:25 000
1975	Topographic map	1:25 000
1982	Topographic map	1:25 000
1988	Topographic map	1:25 000
2006	Topographic map	1:25 000

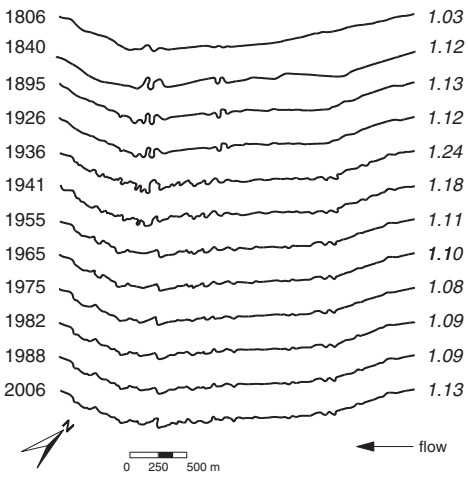

Figure 9. Channel centrelines derived from the 12 topographic historical maps. Values on the right-hand side quantify the sinuosity of the Dutch part of the channel.

A digital elevation model (DEM) was obtained from LiDAR surveys carried out between 1997 and 1998, which covered the entire Dutch part of the study area (Actueel Hoogtebestand Nederland, AHN; Van Heerd *et al.*, 2000). The LiDAR data resolution amounted to 1 point per 4 m^2 with a vertical accuracy of 0.20 m and a horizontal accuracy of 0.30 m. Outliers, vegetation and buildings were removed from the dataset to ensure the data represent the actual Earth surface. The data were interpolated on a grid with a 1 m resolution, using linear interpolation. The DEM was used to identify the valley edges as shown in Figure 4, and to make an estimate of the valley incision since the construction of the channel.

In addition to the historical and remotely sensed data described above, field data were collected. In a first reconnaissance survey, traces of iron oxide and gravel layers in the sedimentary succession were found at several locations along the valley edge (Figure 5). Sedimentary successions were described at 10 locations along the valley edge where the sediment was exposed. Figure 3d, g show examples of these exposed terrace deposits. These 10 exposed locations were not evenly distributed over the valley length. Therefore, 49 cores were subsequently collected along the entire length of the valley to establish the spatial distribution of sediment properties. A hand auger was used for drilling down to 2.2 m below ground level. The depth of iron oxide layers in the profile was recorded at each location. A distinction was made between profiles consisting solely of sand and profiles where gravel layers were present in the profile, in which the gravel layer depth was recorded as well. This resulted in an along-valley view on traces of groundwater seepage and gravel.

Results

Valley incision

Figure 10 shows the DEM of the study area including the 2006 channel centreline. Several geomorphological units discussed earlier can be recognized in this figure. Near the German border, a Rhine terrace remnant (B) borders the channel at its northern side. Moving in the downstream direction, a gentle westward slope of the land surface surrounding the channel is part of the Meuse terrace, also shown in Figure 1c. The most distinctive features are the parabolic sand dunes near the confluence with the river Meuse (A). These aeolian sand dunes date from the Younger Dryas period, approximately 12 000 years ago (Van den Berg, 1996). The dunes consist of coarse-grained sand and show local elevation differences up to 20 m. The LiDAR data show the aeolian dunes have a larger extent than indicated in Figure 1, which was based on Stiboka (1975), indicating the accuracy limitations of the latter report.

When focusing on the area near the channel, the most notable feature in Figure 10 is the incised valley near the confluence with the river Meuse. The DEM shows the channel has incised over several metres (see also the upper part of Figure 12).

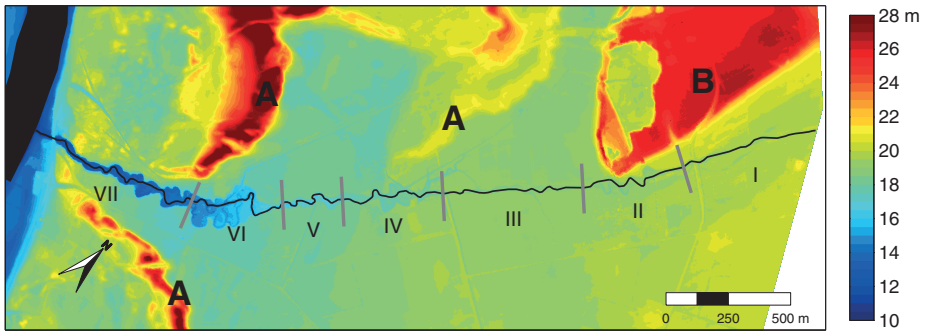

Figure 10. Digital elevation model of the study area, including the centreline of the channel in 2006. Elevation is shown in metres above mean sea level. Several geomorphological units are indicated, i.e. the parabolic sand dunes near the confluence with the river Meuse (A) and a Rhine terrace near the German border (B). The roman numerals label the sections indicated in Figure 12. This figure is available in colour online at wileyonlinelibrary.com/journal/espl

From historical maps it was possible to extract the valley edge, as shown for example in Figure 8. The first topographic map, dating from 1806, did not show any feature that would suggest the presence of a valley edge. From 1840 onwards, all maps depict valley edges, as illustrated in Figure 11. The map of 1926 did not show any change in the location of the valley edge compared to 1895. Also, no changes are observed in the period from 1955 to 2006. Note that the valley edge of 1997 is derived from the LiDAR dataset, which includes much more detail than the valley edges derived from the historical maps.

Figure 11 shows that until 1840 the valley incision was concentrated in the reach downstream of the first meander (section VI), because upstream of that location no valley edges were drawn. The map of 1895 shows that the extent of the valley incision reached up to section IV. From 1936 onwards, the knickpoint location and valley width in the downstream reach of the Nierskanaal were constant, suggesting the valley incision to be stable in that period.

The top panel in Figure 12 shows the present longitudinal valley bottom profile. The valley bottom profile in the upstream part runs largely parallel to the valley edge, whereas the valley bottom in the downstream part becomes progressively deeper downstream. This pattern cannot be readily explained as a response to a draw-down curve of the channel bed level, creating erosion that progressively retreats in the upstream direction. The valley bottom profile has a bilinear shape with a knickpoint around 1.5 km from the Dutch–German border. Earlier we showed that the present extent of the valley incision has been stable since the mid 1930s (Figure 11). Because the knickpoint coincides with the most upstream extent of the valley incision, we can assume that the knickpoint has also been stable ever since the 1930s.

Several processes played a role during the process of valley incision. Figure 3c shows the presence of overland flow within the incised valley during one of the field surveys, caused by water that was seeping out of the valley wall. The upper part of Figure 12 shows where an iron oxide layer was recorded, and at what depth. Iron oxide was found in almost all cores in the deeply incised part of the valley. The shape of the incision in this section shows similarities with so-called amphitheatre-shaped canyons (Kochel and Piper, 1986; Howard and McLane, 1988; Schumm *et al.*, 1995), which are typically attributed to erosion by local seepage flow. The average depth where the iron oxide was found was 1.4 m below the level of the valley edge. Considering the current channel depth (1.2 m), this could have been below the constructed channel bed before incision. We argue that seepage has been triggered by valley incision, which in turn may have accelerated valley incision. Both seepage and meander dynamics may have contributed to the width of the incised valley. Seepage increases the moisture content of the valley wall, which enhances bank erosion at locations where the meander banks encounter the valley wall. This has resulted in a present-day valley depth up to 9 m and a valley width up to 170 m, or 19 times the current channel width.

The knickpoint in the bed-level profile coincides with the transition from coarse-grained bed sediment in the upstream part of the channel, and gravel in the downstream part (Figure 3a, b). Results from the 49 cores (Figure 12) reveal that in the valley wall two gravel layers are present, located upstream and downstream of the knickpoint in the valley bottom. The progressive retreat of the valley edge, illustrated in Figure 11, shows that it is likely that valley incision has initiated in the downstream reach and progressively proceeded in the upstream direction. This process will have continued until the gravel layer was reached, which consists of particles

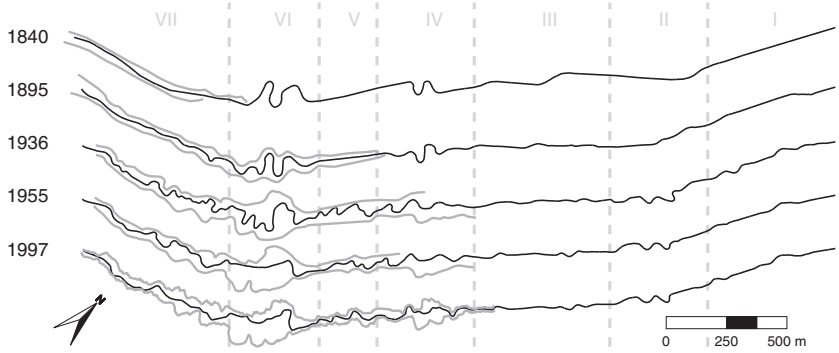

Figure 11. Evolution of the channel centreline (black) and valley edge (grey). The valley edges from 1840, 1895, 1936 and 1955 are derived from topographic maps. The valley edge of 1997 is derived from the LiDAR dataset. The roman numerals label the sections indicated in Figure 12.

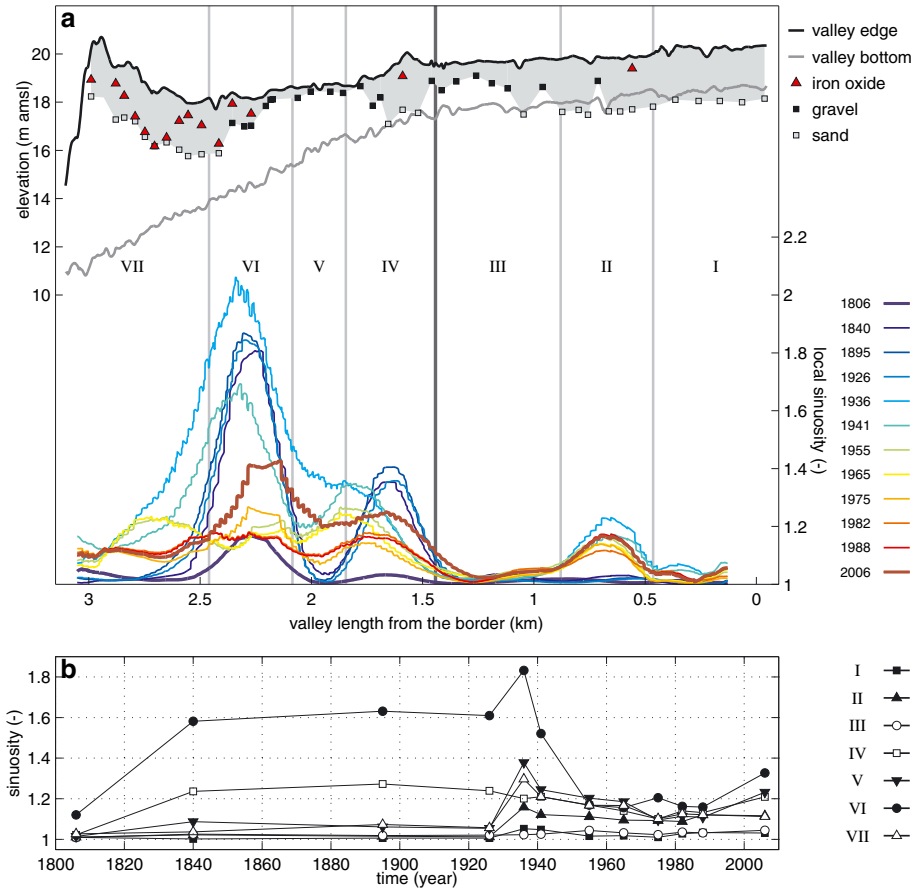

Figure 12. Longitudinal (a) and temporal (b) variability of local sinuosity. Right vertical axis in panel (a): spatiotemporal variation of local sinuosity along the valley axis for all 12 historical channel centrelines. Local sinuosity is determined with a window-size of 250 m. Left vertical axis in panel (a): elevation of the valley edge and valley bottom in metres above mean sea level. The upper part of the figure shows the locations of cores, with a maximum depth of 2.2 m below the level of the valley edge. Red triangular markers indicate locations where traces of iron oxide were found, solid black squares correspond to locations where the hand auger reached a gravel layer, and delineated squares indicate the deepest point to which the hand auger reached in a sand layer. The grey zone marks the coring depth and the extent of the sand deposits. This figure is available in colour online at wileyonlinelibrary.com/journal/espl

too coarse to be readily transported. From then onward, the valley incision will have been retarded, which may have been amplified by spreading of the gravel over the channel bed by the flow. The deposited gravel can act as an armouring layer, increasing the erosion resistance of the channel bed. The established changes in water levels in the river Meuse may also have had an effect on the incision rate of the valley. Both the presence of gravel on the channel bed and raised water levels in the river Meuse will have counteracted valley incision.

Meander dynamics

Spatial series of the local sinuosity are determined to discuss the meander dynamics of the channel over the past 240 years. Local sinuosity, denoted by S_{local}, was obtained by dividing the channel length within a moving window by a predefined length along the valley centreline. The moving window is 250 m long, which is roughly equal to three meander wavelengths.

Figure 12a shows spatial series of the local sinuosity for all 12 historical channel centrelines. The results from the 49 cores along the valley are included in the figure, and the elevation of the valley edge and valley bottom are indicated, as well. The valley edge runs nearly horizontally in downstream direction until 1.5 km from the German–Dutch border. The increase in slope marks the transition between two Meuse terraces. Downstream of the transition, the valley edge again runs nearly horizontal. Near the outlet to the river Meuse, the peak in the surface level reflects the aeolian sand dunes in the area.

Figure 12b shows the temporal variability of the local sinuosity in each of the seven sections defined in Figure 12a. The 1806 channel centreline shows meandering has initiated in section VI, where sinuosity increased rapidly in time up to a maximum of around 2. Figure 11 shows that, in this section, meandering had initiated before valley incision had started. Meandering also initiated in section IV, in the period between 1806 and 1840. Both in section IV and in section VI, meandering developed independently, at least until 1926. From 1936 onwards, sections IV and VI had merged, which is reflected in an increase in sinuosity in section V.

Several meander cutoff events have occurred between 1926 and 1955. The remainders of those are shown in Figure 10, e.g. in section VI. Meander cutoffs result in a decrease in sinuosity. In section IV, cutoff events have occurred between 1926 and 1936. Most evident are the cutoff events in section VI. Figure 12b clearly shows a decrease of local sinuosity between 1936 and 1955. For both sections IV and VI, it can be concluded that the cutoff events are clustered within a 10- to 20-year time span. Using the meander model of Howard and Knutson (1984), Stølum (1996) showed from numerical simulations that cutoff events tend to cluster. This was subsequently confirmed by field research by Stølum (1996), who concluded that each cutoff has a tendency to trigger other cutoffs in its vicinity by causing accelerated local change. This explains the cutoff clustering in space and time as observed.

The upstream sections of the channel show little activity over the past 240 years. In section II, meandering has initiated between 1926 and 1936. The sinuosity in section II does not show any significant changes after 1936 (Figure 12b), which can be attributed to the construction of bank revetments between 1900 and 1940. Bank protection, albeit left unmaintained (see Figure 3e), may have prevented the channel from active meandering in the upper sections.

The valley bottom profile confirms the existence of a difference in morphodynamic behaviour between sections III and IV. Figure 12 shows a knickpoint at the boundary between the inactive upstream sections I through III, and the active downstream sections IV through VII. Both the upstream part and the downstream part show a nearly constant slope. The two parts may have developed to reach two alternative states of a morphological equilibrium, pertaining to laterally confined conditions and a more natural state with erodible banks, respectively.

Initiation of meandering

Figure 10 shows the current meandering planform including the DEM of the surrounding Earth surface. Sections II, IV and VI, where meandering has initiated, are located in the direct vicinity of elevated sedimentary units, i.e. aeolian sand dunes and a Rhine terrace remnant. Each of the three hotspots for meander initiation coincides with the toe of a topographic high. Figure 12 shows that iron oxide was found in the Pleistocene terrace deposits at those spots, which is related to lateral groundwater seepage flows (Anderson, 1988). While it remains unknown whether seepage was present before the channel was constructed, it is likely that groundwater levels in the study area were affected by the construction of the channel.

In flat terrains, precipitation usually infiltrates the soil vertically. The vicinity of a terrace remnant or an aeolian dune, however, changes the groundwater flow in the surroundings of the channel. A topographic high causes the groundwater to flow in a lateral direction away from the elevated terrain, causing groundwater seepage in lower parts of the landscape, e.g. valleys. Seepage through the valley walls increases the moisture content of the bank. Field research (Wilson *et al.*, 2007; Fox *et al.*, 2007; Van Balen *et al.*, 2008) and laboratory studies (Fox *et al.*, 2006; Lindow *et al.*, 2009; Fox and Wilson, 2010) have shown a positive correlation between seepage flow and bank instability and erodibility.

Results from the cores confirmed that iron oxide is present in the banks at each of the three spots of meander initiation, but occurred also in section VII. In the latter section, we relate the seepage with the relatively deep valley incision, which we described earlier. In sections II, IV and VI iron oxide was found close to the level of the valley edge (<1 m). This provides a clue that seepage has triggered meander initiation. The upper part of Figure 12 also shows that, especially in sections II and IV, and to some extent also in section VI, the subsurface mainly consists of sand. The subsurface of both sections III and V mainly consist of gravel. We conclude that meandering in the channel under study has initiated in channel reaches with a floodplain consisting of sand, at spots in the vicinity of topographic highs, where local seepage flow causes seepage erosion and enhances the erodibility of the banks, promoting fluvial erosion.

Conclusions

The objective of this study was to contribute to the knowledge about the role of floodplain heterogeneity on meander formation, by making a historical reconstruction of the development of an initially straight channel. A historical reconstruction was made of a channel constructed in the 18th century between the rivers Niers and Meuse, on the Dutch–German border. Within the Dutch part of the channel, meandering has initiated at three locations. The upstream part of the channel did not show any meander dynamics after the first meander had initiated, because of bank protection. Downstream of the protected bank area, the channel evolved into an actively meandering channel, featuring meander cutoffs.

From field evidence it appears that the sections of the channel where meandering has initiated correspond to sections of the channel where iron oxide was found within 1 m from the surface level, indicating groundwater seepage. The groundwater seepage originates from the banks and valley sides adjacent to higher elevated terrains, composed of terrace remnants and aeolian sand dunes. Since the subsurface of these sections mainly consists of sand, local seepage flow causes seepage erosion and enhances the erodibility of the banks, promoting fluvial erosion. The resulting bank erosion may have resulted in small perturbations in the channel planform. These perturbations in the initial planform, in turn, are the most plausible trigger for the initiation of meandering in this case study.

Meandering has initiated in three separate sections of the channel. The spatial variation in meander initiation was attributed to local differences in hydrology (seepage) and geology (presence of gravel). Recently, meander research has focused on the role of floodplain heterogeneity on meander dynamics, e.g. local differences in hydrology and geology. Commonly, a constant erosion coefficient is used for the whole river reach to parametrize bank erosion. The present study shows that spatial heterogeneities may assert a strong control over sinuosity developments over two centuries of planform change. These observations justify efforts to implement the influence of floodplain heterogeneity and the effect of seepage on bank erosion in meander models.

Acknowledgements—This study is part of a research project funded by the STOWA, the Foundation for Applied Water Research (project 443209). The authors would like to thank Hans de Mars from Royal Haskoning for coming up with the initial story on this remarkable channel. We also like to thank Water Board Peel & Maasvallei for providing the GPS survey data, the German Niersverband for providing discharge data and other background information on the channel, and Roel Dijksma and Tineke van der Ploeg for their help, both during fieldwork and during writing of the manuscript. Furthermore, the authors would like to thank Remko Uijlenhoet, the associate editor and five anonymous reviewers for their comments on the manuscript.

References

Abad JD, García MH. 2006. RVR Meander: a toolbox for re-meandering of channelized streams. *Journal of Computers and Geosciences* **31**: 91–101.

Anderson DW. 1988. The effect of parent material and soil development on nutrient cycling in temperate ecosystems. *Biogeochemistry* **5**: 71–97.

Bartley R, Keen RJ, Hawdon AA, Hairsine PB, Disher MG, Kinsey-Henderson AE. 2008. Bank erosion and channel width change in a tropical catchment. *Earth Surface Processes and Landforms* **33**: 2174–2200.

Blondeaux P, Seminara G. 1985. A unified bar-bend theory of river meanders. *Journal of Fluid Mechanics* **157**: 449–470.

Braudrick CA, Dietrich WE, Leverich GT, Sklar LS. 2009. Experimental evidence for the conditions necessary to sustain meandering in coarse-bedded rivers. *Proceedings of the National Academy of Sciences of the United States of America* **106**: 16936–16941.

Callander RA. 1969. Instability of river channels. *Journal of Fluid Mechanics* **36**: 465–480.

Charlton ME, Large ARG, Fuller IC. 2003. Application of airborne LiDAR in river environments: the River Coquet, Northumberland, UK. *Earth Surface Processes and Landforms* **28**: 299–306.

Church M, Rice SP. 2009. Form and growth of bars in a wandering gravel-bed river. *Earth Surface Processes and Landforms* **34**: 1422–1432.

Coulthard TM, Van de Wiel MJ. 2006. A cellular model of river meandering. *Earth Surface Processes and Landforms* **31**: 123–132.

Crosato A. 1987. Simulation model of meandering processes of rivers. In *Extended Abstracts of the International Conference*: *Euromech 215 – Mechanics of Sediment Transport in Fluvial and Marine Environments*, European Mechanics Society, Santa Margherita Ligure, Genoa, Italy; 158–161.

Crosato A. 2007. Effects of smoothing and regridding in numerical meander migration models. *Water Resources Research* **43**: W01401.

De Moor JJW, Verstraeten G. 2008. Alluvial and colluvial sediment storage in the Geul River catchment (The Netherlands): combining field and modelling data to construct a Late Holocene sediment budget. *Geomorphology* **95**, 487–503.

Engelund F. 1970. Instability of erodible beds. *Journal of Fluid Mechanics* **42**: 225–244.

Federici B, Paola C. 2003. Dynamics of channel bifurcations in noncohesive sediments. *Water Resources Research* **39**: 1162.

Fox GA, Wilson GV. 2010. The role of subsurface flow in hillslope and stream bank erosion: a review. *Soil Science Society of America Journal* **74**: 717–733.

Fox GA, Wilson GV, Periketi RK, Cullum RF. 2006. Sediment transport model for seepage erosion of streambank sediment. *Journal of Hydrologic Engineering* **11**: 603–611.

Fox GA, Wilson GV, Simon A, Langendoen EJ, Akay O, Fuchs JW. 2007. Measuring streambank erosion due to ground water seepage: correlation to bank pore water pressure, precipitation and stream stage. *Earth Surface Processes and Landforms* **32**: 1558–1573.

Friedkin JF. 1945. A laboratory study of the meandering of alluvial rivers. US Army Corps of Engineers Waterways Experiment Stations, Vicksburg, MS.

Güneralp I, Rhoads BL. 2011. Influence of floodplain erosional heterogeneity on planform complexity of meandering rivers. *Geophysical Research Letters* **38**: L14401.

Hansen E. 1967. *On the formation of meanders as a stability problem*. Technical Report. Progress Report 13. Coastal Engineering Lab, Technical University of Denmark.

Hooke JM, Yorke L. 2010. Rates, distributions and mechanisms of change in meander morphology over decadal timescales, River Dane, UK. *Earth Surface Processes and Landforms* **35**: 1601–1614.

Howard AD. 1996. Floodplain processes. In *Modelling Channel Evolution and Floodplain Morphology*. Wiley: Chichester; 15–62.

Howard AD, Knutson TR. 1984. Sufficient conditions for river meandering: a simulation approach. *Water Resources Research* **20**: 1659–1667.

Howard AD, McLane CF. 1988. Erosion of cohesionless sediment by groundwater seepage. *Water Resources Research* **24**: 1659–1674.

Ikeda S, Parker G, Sawai K. 1981. Bend theory of river meanders. Part 1. Linear development. *Journal of Fluid Mechanics* **112**: 363–377.

Johannesson H, Parker G. 1989. Linear theory of river meanders. In *River Meandering*. Water Resources Monograph, Vol. **12**. American Geophysical Union: Washington, DC; 181–214.

Kasse C, Hoek WZ, Bohncke SJP, Konert M, Weijers JWH, Cassee ML, van der Zee RM. 2005. Late Glacial fluvial response of the Niers–Rhine (western Germany) to climate and vegetation change. *Journal of Quaternary Science* **20**: 377–394.

Kochel RC, Piper JF. 1986. Morphology of large valleys on Hawaii: Evidence for groundwater sapping and comparisons with Martian valleys. *Journal of Geophysical Research* **91**: 175–192.

Langendoen EJ, Alonso CV. 2008. Modeling the evolution of incised streams. I. Model formulation and validation of flow and streambed evolution components. *Journal of Hydraulic Engineering* **134**: 749–762.

Langendoen EJ, Simon A. 2008. Modeling the evolution of incised streams. II: Streambank erosion. *Journal of Hydraulic Engineering* **134**: 905–915.

Lindow N, Fox GA, Evans RO. 2009. Seepage erosion in layered stream bank material. *Earth Surface Processes and Landforms* **34**: 1693–1701.

Motta D, Abad JD, Langendoen EJ, García MH. 2012a. A simplified 2D model for meander migration with physically-based bank evolution. *Geomorphology* **163–164**: 10–25.

Motta D, Abad JD, Langendoen EJ, García MH. 2012b. The effects of floodplain soil heterogeneity on meander planform shape. *Water Resources Research* **48**: W09518.

Nienhuis PH. 2008. *Environmental History of the Rhine–Meuse Delta*: *An Ecological Story on Evolving Human–Environmental Relations Coping with Climate Change and Sea-Level Rise*. Springer: Berlin.

Notebaert B, Verstraeten G, Govers G, Poesen J. 2009. Qualitative and quantitative applications of LiDAR imagery in fluvial geomorphology. *Earth Surface Processes and Landforms* **34**: 217–231.

Peakall J, Ashworth PJ, Best JL. 2007. Meander-bend evolution, alluvial architecture, and the role of cohesion in sinuous river channels: a flume study. *Journal of Sedimentary Research* **77**: 197–212.

Pišút P. 2002. Channel evolution of the pre-channelized Danube River in Bratislava, Slovakia (1712–1886). *Earth Surface Processes and Landforms* **27**: 369–390.

Richardson WR. 2002. Simplified model for assessing meander bend migration rates. *Journal of Hydraulic Engineering* **128**: 1094–1097.

Schumm SA, Khan HR. 1971. Experimental study of channel patterns. *Nature* **233**: 407–409.

Schumm SA, Boyd KF, Wolff CG, Spitz WJ. 1995. A ground-water sapping landscape in the Florida Panhandle. *Geomorphology* **12**: 281–297.

Seker DZ, Kaya S, Musaoglu N, Kabdasli S, Yuasa A, Duran Z. 2005. Investigation of meandering in Filyos River by means of satellite sensor data. *Hydrological Processes* **19**: 1497–1508.

Smith CE. 1998. Modeling high sinuosity meanders in a small flume. *Geomorphology* **25**: 19–30.

Stiboka. 1975. *Bodemkaart van Nederland, Schaal 1:50000*. Technical Report. Stichting voor Bodemkartering, Wageningen.

Stølum HH. 1996. River meandering as a self-organized process. *Science* **271**: 1710–1713.

Struiksma N, Olesen KW, Flokstra C, De Vriend HJ. 1985. Bed deformation in curved alluvial channels. *Journal of Hydraulic Research* **23**: 57–79.

Sun T, Meakin P, Jøssang T, Schwarz K. 1996. A simulation model for meandering rivers. *Water Resources Research* **32**: 2937–2954.

Sun T, Meakin P, Jøssang T. 2001. A computer model for meandering rivers with multiple bed load sediment sizes. *Water Resources Research* **37**: 2227–2241.

Timár G, Székely B, Molnár G, Ferencz C, Kern A, Galambos C, Gercsák G, Zentai L. 2008. Combination of historical maps and satellite images of the Banat region: re-appearance of an old wetland area. *Global and Planetary Change* **62**: 29–38.

Uribelarrea D, Pérez-González A, Benito G. 2003. Channel changes in the Jarama and Tagus rivers (central Spain) over the past 500 years. *Quaternary Science Reviews* **22**: 2209–2221.

Van Balen RT, Kasse C, De Moor J. 2008. Impact of groundwater flow on meandering: example from the Geul River, The Netherlands. *Earth Surface Processes and Landforms* **33**: 2010–2028.

Van den Berg MW. 1996. Fluvial sequences of the Maas: a 10 Ma record of neotectonics and climate change at various time-scales. PhD thesis, Landbouwuniversiteit Wageningen, The Netherlands.

Van Dijk WM, Van de Lageweg WI, Kleinhans MG. 2012. Experimental meandering river with chute cutoffs. *Journal of Geophysical Research* **117**: F03023.

Van Dongen B, Meijer D. 2008. *Zomerbedbodemveranderingen van de Maas (1889–2007)*. Technical Report. Rijkswaterstaat Dienst Limburg.

Van Heerd RM, Kuijlaars EAC, Teeuw MP, van't Zand RJV. 2000. *Productspecificatie AHN 2000*. Technical Report MDTGM 2000.13. Rijkswaterstaat, Adviesdienst Geo-informatie en ICT, Delft.

Warburton J, Danks M, Wishart D. 2002. Stability of an upland gravel-bed stream, Swinhope Burn, Northern England. *Catena* **49**: 309–329.

Wilson GV, Periketi RK, Fox GA, Dabney SM, Shields FD, Cullum RF. 2007. Soil properties controlling seepage erosion contributions to streambank failure. *Earth Surface Processes and Landforms* **32**: 447–459.

Wolfert HP. 2001. Geomorphological change and river rehabilitation. PhD thesis, Wageningen University and Research Centre, The Netherlands.

Wolfert HP, De Lange GW. 1990. *Toelichting op kaartblad 52 Venlo*; *Geomorfologische kaart van Nederland 1:50 000*. Technical Report. Staring Centrum, Wageningen/Rijks Geologische Dienst, Haarlem.

Zolezzi G, Seminara G. 2001. Downstream and upstream influence in river meandering. Part 1. General theory and application to overdeepening. *Journal of Fluid Mechanics* **438**: 183–211.